J Low Temp Phys (2009) 156: 71–83
DOI 10.1007/s10909-009-9890-2

Drag Measurement on an Oscillating Sphere in Helium II

A.M. Hemmati · S. Fuzier · E. Bosque · S.W. Van Sciver

Received: 30 March 2009 / Accepted: 17 May 2009 / Published online: 4 June 2009
© Springer Science+Business Media, LLC 2009

Abstract Here we report measurement of the drag on a 3 mm oscillating sphere in superfluid ^{4}He in the temperature range 1.6 K to 2.1 K. A Nb-Ti superconducting solenoid is used to suspend a niobium sphere; meanwhile a similar superconducting quadrupole magnet centers and helps to stabilize the ball at one location in the flow channel. The niobium sphere is levitated by the superconducting magnetic suspension system; then the oscillation is obtained by dropping the ball from one equilibrium point to a lower equilibrium point via reducing the levitating magnetic field. The sphere's oscillation is then recorded with a high-speed CCD camera. The velocity of the sphere is obtained by comparing the images captured and the distance the sphere has moved with time. Drag force is calculated through its relation to the maximum velocity decay rate. The sphere is contained within a closed end channel that allows measurements in liquid or gaseous helium and vacuum.

Keywords Drag measurement · Magnetic suspension · He II turbulence

1 Introduction

1.1 Drag Coefficient

The force of drag as an object moves through a fluid has been known for many years. Drag force is an opposing force that the fluid exerts on an object in a direction opposite to its motion. The drag coefficient is a non-dimensional value that relates the drag force to the fluid velocity and body's shape and size and is defined by the following

A.M. Hemmati · S. Fuzier · E. Bosque · S.W. Van Sciver (✉)
Department of Mechanical Engineering, Florida State University, Tallahassee, FL 32305, USA
e-mail: vnsciver@magnet.fsu.edu

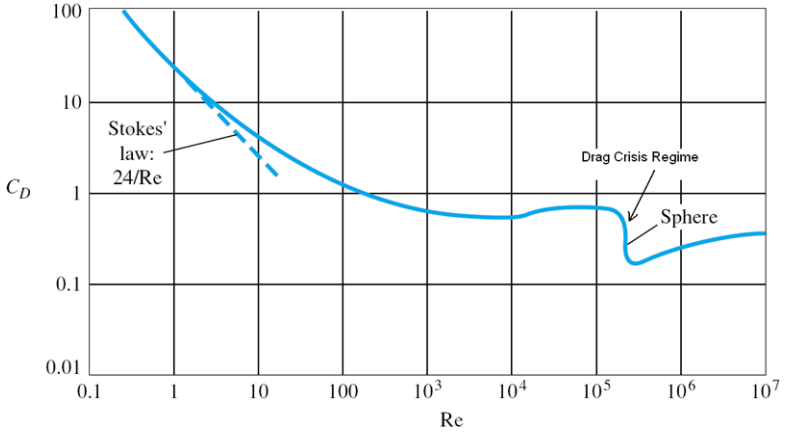

Fig. 1 (Color online) Sphere drag coefficient versus Reynolds number for classical fluid [4]

equation,

$$C_D = \frac{F_D}{\frac{1}{2}\rho A v^2} \tag{1}$$

where ρ is fluid density, v is fluid velocity, A can differ based upon object but for sphere is the frontal area, and F_D is the drag force.

The drag coefficient is the parameter that characterizes the behavior of the drag force on a body. There are numerous experiments that have been done to determine the drag coefficient of many different shapes in terms of Reynolds number; where Reynolds number is defined as,

$$\mathrm{Re} = \frac{\rho v D}{\mu} \tag{2}$$

where v is fluid velocity, D is characteristic diameter, and μ is viscosity. Reporting drag versus Reynolds number is a way to scale all the measurements of drag and makes it simple to compare different drag measurements independent of the medium.

The determination of drag coefficient plays an extremely important role in design of airplanes, automobiles, boats, and many more vehicles. For certain applications such as jet airplanes and extremely high speed vehicles that go into very high Reynolds numbers, full scale testing can become difficult and costly. Liquid helium has kinematic viscosity much smaller than air (nearly three orders of magnitude); therefore, testing in helium for the same or smaller scale models can provide solutions to high Reynolds number problems [1].

The drag coefficient for flow around a sphere has been studied extensively [2]. Figure 1 displays normal behavior for a drag coefficient of sphere versus Reynolds number. An equation given by White [3] that offers a fit for the drag coefficient of a sphere in laminar regime, before the "drag crisis" for Reynolds number range of $0 \leq \mathrm{Re} \leq 2 \times 10^5$ is given as,

$$C_D \approx \frac{24}{\mathrm{Re}} + \frac{6}{1+\sqrt{\mathrm{Re}}} + 0.4 \tag{3}$$

Equation (3) has an accuracy of ±10%. In the crisis regime the wake behind the sphere thins due to the turbulent boundary layer, and so the drag is reduced. In this experiment, we are interested in drag on a sphere in He II.

1.2 He II

Helium has the lowest critical point of all fluids, $T_c = 5.2$ K, and $P_c = 0.226$ MPa. Liquid helium can exist in two completely different phases, He I and He II, and since it does not solidify at low temperatures without an external pressure of more than 2.5 MPa, it has no triple point. He I, the high temperature phase, is known to behave as a classical fluid. The line that separates He I and He II on the phase diagram is called the λ-*line*. The λ-*point* at 2.176 K is the transition at saturated vapor pressure with the transition temperature continuing to decrease as pressure is increased. He II is classified as a quantum fluid because it has properties including its fluid dynamics that can only be understood in terms of quantum mechanics.

To understand some of the unique characteristics of He II, Tisza (1938) and Landau (1941) developed a theory of He II as a fluid composed of two components [5]. In the two-fluid model He II can be thought as consisting of two interpenetrating fluids, normal fluid and superfluid, which have temperature dependent densities and are fully miscible. These two components describe the dynamics of He II under a temperature or pressure gradient. The normal fluid is assumed to behave as a classical fluid and have a density ρ_n, viscosity μ_n, and entropy s_n. Although the superfluid part has a density ρ_s, it has zero viscosity, and zero entropy. Therefore, all the entropy in He II is carried by the normal fluid component. Then, average heat current can be given as,

$$q = \rho_n s_n T \langle v_n \rangle \tag{4}$$

where, v_n is normal fluid velocity. The total density of He II is the addition of densities of both normal fluid and superfluid components and is given as,

$$\rho = \rho_n + \rho_s \tag{5}$$

with the momentum of the fluid given as,

$$\rho v = \rho_s v_s + \rho_n v_n \tag{6}$$

The dynamics of He II display a number of unique characteristics. Flow of the viscous normal fluid component can be generated by a net heat current, (4), while the superfluid component conserves momentum consistent with (6). Above a certain velocity, the normal fluid component should become turbulent based on classical Reynolds number criteria. Turbulence in the superfluid component manifests itself as quantized vortices distributed throughout the bulk fluid. In this combined turbulent state, there is the mechanism of mutual friction between the two fluid components that controls the heat transport and can couple the two fluid components together under forced flow conditions. This latter mechanism is what leads to the classical-like friction in high Reynolds number fluid dynamics [7].

1.3 Drag in He II

Since He II has exceptional and non-classical behavior, it is a unique fluid displaying unique characteristics. The question is to what extent the properties of He II compare to those of classical fluids? One of these properties is the drag coefficient on a sphere. In classical fluids, there are correlations that can predict the drag coefficient on a sphere for Reynolds number $\mathrm{Re} < 10^5$ with an average of 10% error for example as presented in (3). An important goal would be to develop a similar condition to estimate the drag coefficient for He II.

The drag on a sphere in He II has only been studied by a few researchers [6–10]. Most of these studies have involved either using an external device attached to the sphere to suspend it in the flow field, or simply releasing the sphere to fall freely at its terminal velocity. Smith *et al.* [6] studied the drag on a 10 mm diameter sphere suspended in a 40 mm channel by small capillary tubes that also acted as pressure taps. They used the pressure distribution over the sphere to compute the drag coefficient and were able to observe the drag crisis in the range of Reynolds number $10^5 \leq \mathrm{Re} \leq 10^6$ in both He I and He II. No significant difference was observed between the two results.

Schoepe and his colleagues [8] performed a drag measurement on an oscillating magnetic sphere of diameter of about 100 μm suspended between niobium plates. They report a drag coefficient similar to that of classical fluid in the turbulent regime of He II, although the main experiment was conducted at 1 K and below, and also in laminar regime. Schoepe *et al.* obtained, for these ranges of temperatures and Reynolds numbers, behavior that does not coincide with that of classical fluids.

Overall, experimental results that have reported the drag coefficient in He II in turbulent regimes or for that matter friction factor measurements in pipe flow have displayed classical-like behavior. For the most part, this observation is based on the argument that at higher velocities both normal and superfluid components are in the turbulent state and in this state both components couple due to mutual friction and this coupling makes the two fluids move together as if they were a classical fluid.

2 Experimental Setup

The present experiment is designed to measure the damping of an oscillating sphere in low temperature helium. The main objective of this experiment is to measure the drag force on the sphere in He II. To achieve this measurement, it is both necessary to have a method of suspending the sphere in the flow field while simultaneously measuring its velocity. Our technique involves suspending a perfectly diamagnetic niobium sphere in a magnetic trap and measuring its velocity using visualization techniques. This method has an advantage in that the sphere is not in contact with any physical objects that can create their own drag and interfer with the measurement. Moreover, this technique provides a unique way to look at how spheres oscillate and move in low temperature helium, gas or liquid.

Since the magnetic field changes at every point in the channel, the disadvantage of a magnetic suspension system are the complications with changing magnetic forces

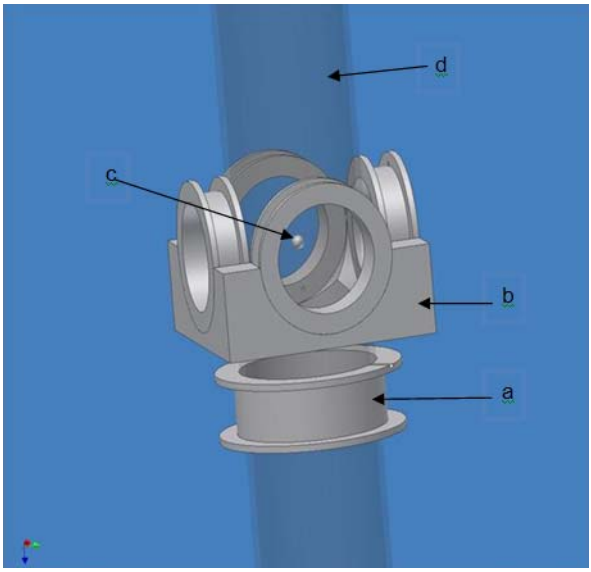

Fig. 2 (Color online) Schematic of magnetic trap with niobium sphere. The sphere, c, is lifted up by the launching solenoid, a, and centered and levitated by quadrupole magnets, b. The quartz channel, d, is on the axis of the coils

and the effect of these forces on an oscillating diamagnetic sphere. In the following section, we describe how these issues have been resolved in the present case.

There are four major components that make up the experimental system. They are: (a) the launching superconducting solenoid; (b) quadrupole magnets; (c) a niobium sphere; and (d) the quartz channel that holds the magnets and the sphere. Figure 2 is a drawing of these parts put together.

2.1 Niobium Sphere

For this experiment a 3 mm $\pm$ 0.005 mm niobium sphere is used as the object of levitation. It is made out of pure niobium and mass of 121 mg. Niobium has lower critical field of 0.25 T and a density of 8570 kg/m^3. The sphere was purchased from United States Ball Corp [11]. The reason for using niobium sphere is that it becomes superconducting at 9.2 K, well above liquid helium temperature, and its specific gravity is low enough that it can be levitated by a modest magnetic field.

2.2 Launching Solenoid

Copper-niobium titanium wire, purchased from SUPERCON Inc, was used to build both the launching solenoid and the quadrupole magnet. The wire has a diameter of 0.102 mm (insulated), contains 54 filaments, and it has critical current of approximately 6.8 A at 4.2 K. The launching solenoid's wire is wound around a cylindrical shaped aluminum mandrel. The solenoid has 1200 turns and with 3.15 A of current the maximum magnetic field at its center is 0.034 T. The inner radius is 12.1 mm and the outer radius is 13.8 mm. To optimize the calculation of the solenoid's parameters the length of solenoid was determined to be 8.0 mm. An image of final build of the launching solenoid is shown in Fig. 3.

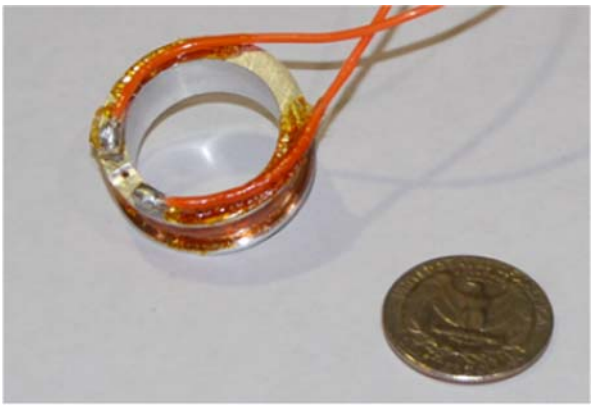

Fig. 3 (Color online) Launching solenoid consisting of 1200 turns of 0.102 mm diameter wire

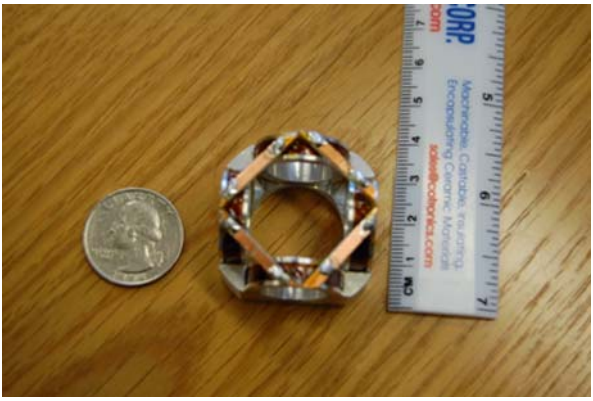

Fig. 4 (Color online) Quadrupole magnet assembly. Each coil consists of 555 turns of 0.102 mm diameter wire

2.3 Quadrupole Magnet

Each of the coils in the quadrupole magnet is designed similarly to the launching solenoid, but with fewer turns and smaller diameter, since a smaller force is sufficient to stabilize the niobium sphere. Each coil of the quadrupole magnet has 555 turn. The inner radius of each of the coils is 8.93 mm, outer radius is 10.6 mm, and length of each coil is 4.00 mm. The center of each coil is located 10.4 mm from the axis of the experiment. Figure 4 is an image of the quadrupole magnet assembly.

2.4 Optical Channel

Two different channels were used for the final assembly for the He II experiment. Channel 1 is an open channel consisting of a quartz tube of inner diameter of 20 mm and outer diameter of 22 mm that supports the magnets and also holds the sphere above the launching solenoid with a circular plug made from G-10. The size of the channel has been determined by requiring that it be at least four times the diameter of the sphere. In the present case the sphere is 3 mm in diameter; therefore, it has minimal effect on the flow cross section as the inner diameter of the channel is 20 mm.

Channel 2 is an improved version built to allow experiments in helium gas or vacuum. This second new channel is a separate vessel that supports the magnets and is immersed in the helium bath. It can be filled with helium by condensing helium gas from a separate gas bottle. This channel is also connected to a vacuum pump, so it is possible to control the amount of helium inside the experiment.

2.5 Final Assembly and Data Acquisition

Once all the parts are ready, with the assembly being similar to Fig. 2, then the whole experimental apparatus is placed inside an optical cryostat. A high speed CCD camera (X-Stream Vision) and a light source (consisting of a incandescent desk lamp) are placed in front of the windows of the cryostat.

The main data obtained from the experiment are video images of the sphere oscillating in the magnetic trap. The aligned camera captures the images and stores them on a computer. The software that is used to do that is called Motion Studio—Image Acquisition and processing from IDT (Integrated Design Tools). Then analysis of these videos is done in Matlab®. A more detailed description of this analysis is provided in a later section.

3 Theory of Measurement

3.1 Magnetic Forces

An exact formula exists to calculate the magnetic field at the center axis of a solenoid (on the axial axis). This equation is denoted by $B_0(z)$, the number zero referring to the axis at the center of the solenoid, and is presented below as,

$$B_0(z) = \frac{\mu_0 * i * n}{2(r_o - r_i)} \left\{ \left(\frac{L_s}{2} + z \right) \ln \left[\frac{\sqrt{r_o^2 + (\frac{L_s}{2} + z)^2} + r_o}{\sqrt{r_i^2 + (\frac{L_s}{2} + z)^2} + r_i} \right] - \left(-\frac{L_s}{2} + z \right) \ln \left[\frac{\sqrt{r_o^2 + (-\frac{L_s}{2} + z)^2} + r_o}{\sqrt{r_i^2 + (-\frac{L_s}{2} + z)^2} + r_i} \right] \right\} \tag{7}$$

where μ_0 is permeability of free space and $\mu_0 = 4\pi \times 10^{-7}$ H/m, i is applied current, L_s is length of solenoid, n is number of turns per length, r_i is inner radius of solenoid, r_o is outer radius of solenoid, and z is some distance away from the center of the solenoid. Furthermore, we used the following equations developed by Dushkin [12] to calculate the radial and axial components of magnetic field of a solenoid at radii other than the center axis. The radial component is used to calculate the force that the quadrupole magnet applies to the sphere on the axis of the channel.

$$B_r(r, z) = -\frac{\mathrm{d}B_0(z)}{\mathrm{d}z} \frac{r}{2} + \frac{\mathrm{d}^3 B_0(z)}{\mathrm{d}z^3} \frac{r^3}{16} \tag{8}$$

From the magnetic field equations, we are able to calculate the external forces acting on the sphere including forces due to buoyancy, and magnetic forces from both launching solenoid and quadrupoles. The force per unit volume due to gravity is given as,

$$F_g = (\rho_{\text{sphere}} - \rho_{\text{He}}) * g \tag{9}$$

and magnetic force per unit volume of launching solenoid is given as,

$$F_s(z) = \frac{1}{\mu_0} B_0(z) \frac{\mathrm{d}B_0(z)}{\mathrm{d}z} \tag{10}$$

and magnetic force per unit volume of the quadrupole magnet is given as,

$$F_q(r) = \frac{16}{\mu_0} B_r(r, z_{\text{const}}) \frac{\mathrm{d}B_r(r, z_{\text{const}})}{\mathrm{d}r} \tag{11}$$

where ρ_{sphere} is the density of the sphere, and ρ_{He} is the density of liquid helium, and z_{const} is the distance that the center of each coil is located from the axis of the experiment and is 10.4 mm. It is also notable to mention that the numerical coefficient 16 in (11) comes from the fact that the radial components of the magnetic field and field gradient are made up of field components of each of four coils.

3.2 Oscillation Experiment

We have developed a one dimensional equation to theoretically map the oscillation of the sphere. This equation is based on a more general one dimensional equation of motion for a sphere in a fluid obtained from Melling [13]. This equation was also used by Zhang [14] to describe the motion of spherical particles in He II. Here we have used the same concept to describe the motion of the niobium sphere given as,

$$\left(\rho_{\text{sphere}} + \frac{\rho_{\text{He}}}{2}\right) \frac{\mathrm{d}^2 z}{\mathrm{d}t^2} = -\frac{3C_d \rho_{\text{He}}}{4d_{\text{sphere}}} \frac{\mathrm{d}z}{\mathrm{d}t} \left|\frac{\mathrm{d}z}{\mathrm{d}t}\right| - K F_M \tag{12}$$

where in our case the body force is made up of two components: the gravitational force plus radial magnetic force given as,

$$F_M = F_g + F_q \tag{13}$$

with z being the direction that the sphere oscillates. d_{sphere} is the sphere diameter and F_M is sum of the magnetic and gravitational forces that is dependent on location of the sphere. F_M does not include the magnetic force of the launching magnet since it is not turned on during the oscillation. K is an empirical force correction factor which in the present case is 2.25. K is derived empirically first by comparing the frequency of the oscillation derived from calculations with frequency observed experimentally. To verify this correction factor, we have used finite element analysis field values obtained from Vector Fields® software to compare our theoretical calculations to predictions by the software. This K-factor corrects the force on the sphere, which is calculated by our equations, and it can also be verified by the software. Such

a correction was expected due to the lack of existence of a unique solution to the magnetic field equations. The value $K = 2.25$ was very consistent throughout all the experiments.

4 Experimental Procedure

The experiment begins by levitating and centering the niobium sphere in an equilibrium position. This same position is maintained for all experiments for consistency reasons. When the sphere is stable, which only takes a few seconds, sphere oscillation is achieved by reducing the current to the bottom magnet to zero. This action causes the sphere to drop down to its lower equilibrium position and oscillate about this new equilibrium point. The damped oscillation is then recorded with the camera.

Data collected in this experiment is completely through high speed digital camera. Once the current to the bottom magnet is quickly decreased to zero, recording of the oscillation begins. One issue that arises during the data collection is the limitation of camera's memory. The data collection can take more than two minutes, and experimentally it was determined that the frequency of the oscillation is 10 to 10.5 Hz. Therefore, to collect more data over longer period of time, it was necessary to come up with a technique to record as much data as possible to capture the decay time and behavior of the oscillation. To resolve this issue, we developed a technique that only captures segments of the oscillation with each segment providing sufficient information about the velocity of the sphere. For the present set of experiments, we determined that to obtain enough data points, we only needed to capture about 0.5 seconds of the oscillation at 100 Hz, which gave us about 50 points of experimental data for each segment.

The image analysis of the data is done by cross correlation codes that we have written in Matlab®. A major part in this analysis is the recognition of the change in position of the sphere one image after another. Once cross-correlation is done between two images a graph can be obtained that provides information about how well the second image matches the first image after it has been moved by a certain number of pixels. This graph has a peak, which can be used to determine the distance the sphere has moved over a certain amount of time. Therefore, by using the known diameter of the sphere as a scale to convert pixels to metric units, and by knowing the frequency and number of frames, we can convert all those images to graphs similar to Fig. 5.

5 Results

Once all the images have been analyzed and converted to data, we can graph these points against the theoretical calculations and from there, estimate the drag coefficient by adjusting C_d to best fit the theoretical curve. We have graphed both experimental velocities and velocities calculated in (12) versus time in Fig. 7. This graph only shows the first section of the data. We determine the drag coefficient for a certain Reynolds number by dividing the whole set of data into number of distinct pieces

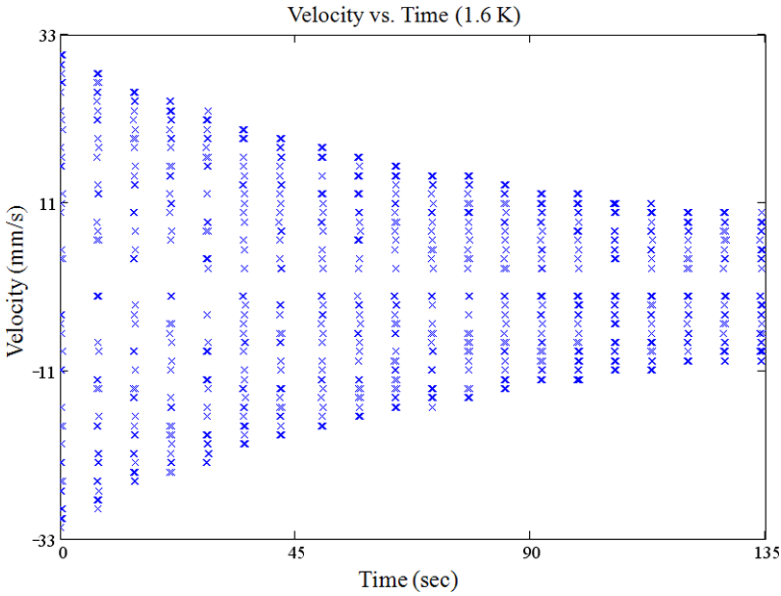

Fig. 5 (Color online) Velocity versus time data collected at 1.6 K

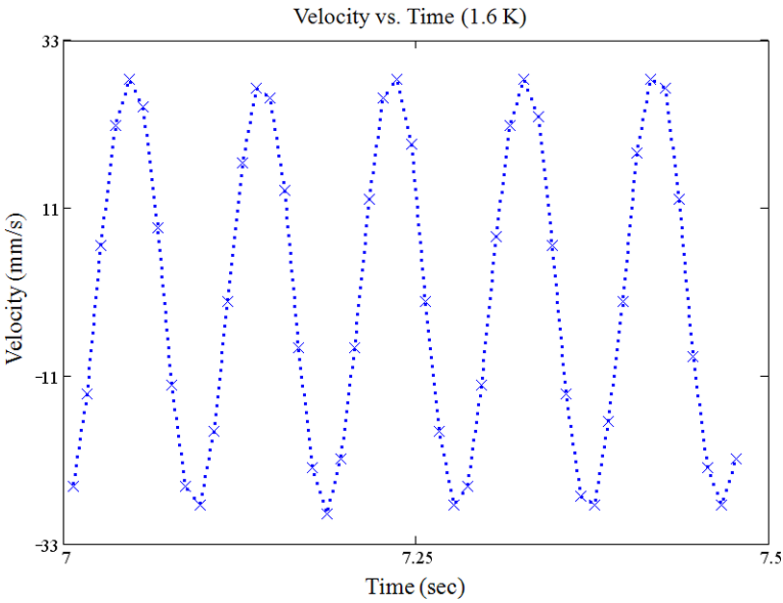

Fig. 6 (Color online) close up of one segment of Fig. 5 with 50 points in 0.5 seconds

(usually 4 or 5). Then, we adjust the drag coefficient value for the theoretical calculations until a best fit is obtained. Changing the C_D by more than $\pm 10\%$ leads to an observable difference between experimental and theoretical curve. The velocity

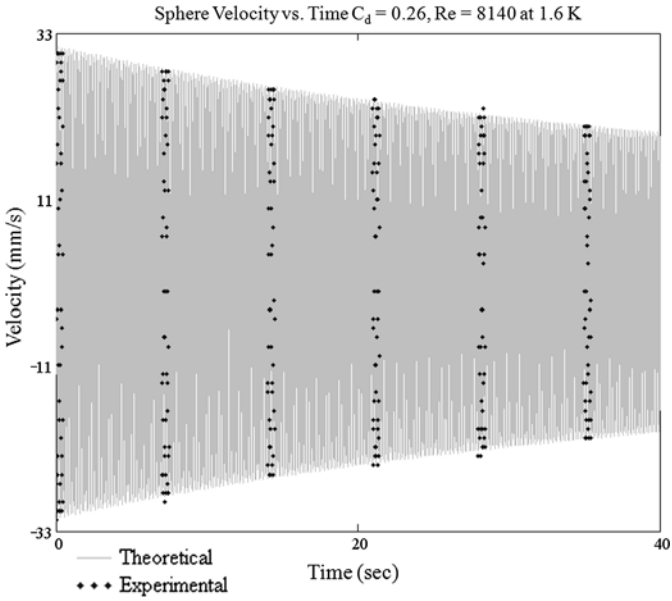

Fig. 7 (Color online) Drag coefficient determination by comparison of experimental data and theoretical data

used to calculate the Reynolds number is based on the average maximum velocity amplitude over the segments that are used in the calculation.

From analyzing these data points we have created a graph of drag coefficient versus Reynolds number which is presented in Fig. 8. These data have been compared to similar measurements of C_d obtained by measuring drag force on spheres moving through He II by Dowley, Firth and Hallett [10] in temperature range of 1.47 K to 2.13 K, and by Smith and Van Sciver [6] at 1.8 K. Also, the line represents the C_d in classical fluids.

To verify that the magnetic forces do not contribute directly to the damping of the sphere oscillation through eddy currents in the coil or coil form, we performed an experiment with the sphere suspended in vacuum. It should be noted that this experiment required some care since the sphere is insulated from the surrounding helium such that the light source easily can heat it above its critical temperature. In this experiment, the sphere oscillation amplitude did not appreciably decay within the duration of the measurement, which was about 200 s. Therefore, we have concluded that the magnetic forces impose no significant additional damping force on the sphere.

6 Conclusions

A successful magnetic suspension system has been built, which is capable of suspending a perfectly diamagnetic sphere for visualization studies. Using this experiment we have measured the drag coefficient in He II in the range of Reynolds number 1000 to 10000. These results suggest that the drag coefficient in He II in the temperature

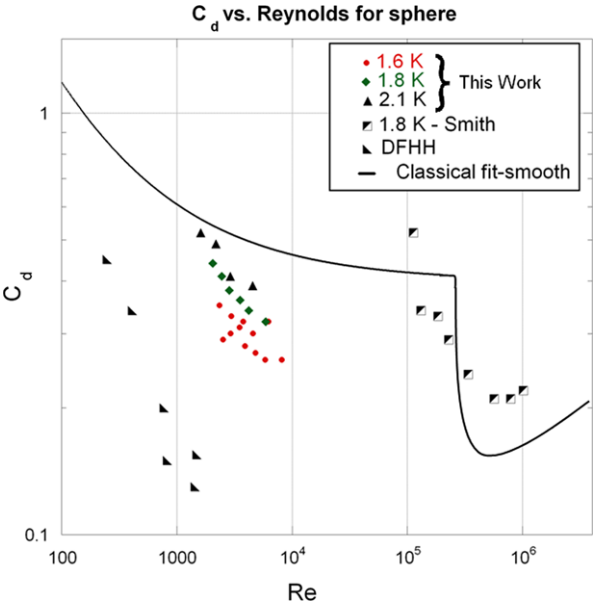

Fig. 8 (Color online) Comparison of C_d versus Reynolds number in He II and classical fluid. Also compared to DFHH, Dowley M.W., Firth D.R. and Hollis Hallett A.C. [10] and Smith M.R. and Van Sciver S.W. [6]

range 2.1 K down to 1.6 K show values reasonably close to classical measurements. Furthermore, the data suggest that there may be small temperature dependence in the drag coefficient measurements. However, additional measurements are required to confirm this observation. By performing this experiment in He I and helium gas, we can verify that our system produces classical values for the drag coefficient.

Acknowledgements We would like to thank Kenneth Pickard for helping with the winding of the magnets, and Russell Wood for helping with the wiring. Tom Dusek helped building the channel. AMH would like to thank Ting Xu for his suggestions with the cross-correlation codes. This work is supported by the National Science Foundation under grant CTS-0729972.

References

1. R.J. Donnelly, Cryogenic fluid dynamics. J. Phys. Condens. Matter **11**, 7783–7834 (1999)
2. H. Schlichting, *Boundary Layer Theory*, 7th ed. (McGraw-Hill Science/Engineering/Math, New York, 1979)
3. F.M. White, *Viscous Fluid Flow*, 1st ed. (McGraw-Hill, New York, 1991), p. 182
4. F.M. White, *Fluid Mechanics*, 4th ed. (McGraw-Hill College, New York, 1998), p. 457
5. S.W. Van Sciver, *Helium Cryogenics*, 1st ed. (Plenum, New York, 1986), p. 101
6. M.R. Smith, S.W. Van Sciver, Measurement of the pressure distribution and drag on a sphere in flowing helium I and helium II. Adv. Cryog. Eng. **43**, 1473–1479 (1998)
7. W.F. Vinen, J.J. Niemela, Quantum turbulence. J. Low Temp. Phys. **128**, 167–231 (2002)
8. M. Niemetz, W. Schoepe, Stability of laminar and turbulent flow of superfluid 4 He at mK temperatures around an oscillating microsphere. J. Low Temp. Phys. **135**(5), 447–469 (2004)
9. R.A. Laing, H.E. Rorschach Jr., Hydrodynamic drag on spheres moving in liquid helium. Phys. Fluids **4**, 564 (1961)
10. M.W. Dowley, D.R. Firth, A.C. Hollis Hallett, in *Proc. 7th Int. Conf. on Low Temperature Physics* (1961)
11. Steel Precision Balls Custom Applications, California. http://www.usball.com/balls/default.html

12. C. Dushkin et al., Magnetic field in a thick superconducting solenoid for dynamic levitation of objects. J. Appl. Phys. **91**(12), 10212–10214 (2002)
13. A. Melling, Tracer particles and seeding for particle image velocimetry. Meas. Sci. Technol. **8**(12), 1406–1416 (1997)
14. T. Zhang, D. Celik, S.W. Van Sciver, Tracer particles for application to PIV studies of liquid helium. J. Low Temp. Phys. **134**(3), 985–1000 (2004). doi:10.1023/B:JOLT.0000013213.61721.51